

Deep Multi-View Clustering via Multiple Embedding

Bingqian Lin^{1†}, Yuan Xie^{2†}, Yanyun Qu^{1*}, Cuihua Li¹

¹Fujian Key Laboratory of Sensing and Computing for Smart City,
School of Information Science and Engineering, Xiamen University, China

²State Key Laboratory of Intelligent Control and Management
of Complex Systems, Institute of Automation, Chinese Academy of Sciences

Abstract

Exploring the information among multiple views usually leads to more promising clustering performance. Most existing multi-view clustering algorithms perform clustering separately: first extracts multiple handcrafted features or deep features, then conducts traditional clustering such as spectral clustering or K-means. However, the learned features may not often work well for clustering. To overcome this problem, we propose the Deep Multi-View Clustering via Multiple Embedding (DMVC-ME), which learns deep embedded features, multi-view fusion mechanism and clustering assignment simultaneously in an end-to-end manner. Specifically, we adopt a KL divergence to refine the soft clustering assignment with the help of a multi-view fused target distribution. The parameters are updated via an efficient alternative optimization scheme. As a result, more clustering-friendly features can be learned and the complementary traits among different views can be well captured. We demonstrate the effectiveness of our approach on several challenging image datasets, where significant superiority can be found over single/multi-view baselines and the state-of-the-art multi-view clustering methods.

Introduction

Multi-view clustering has been intensively studied recently by utilizing the available multi-view information to gather similar subjects into the same group and dissimilar ones into different groups, capturing complementary information and consistency among different views. Usually, the multi-view features are generated by various handcrafted feature extractors. For example, there are many heterogeneous visual features such as SIFT (Lowe 2004), LBP (T. Ojala and Maenpaa 2002), and HOG (Dalal and Triggs 2005). With the development of deep learning, more powerful features can be captured by using various kinds of deep architectures, such as stacked autoencoder (SAE) (P. Vincent and Manzagol 2010), variational autoencoder (VAE) (Kingma and Welling 2014), and convolutional autoencoder (CAE) (Guo X 2017), which were proposed for unsupervised learning. Multi-view features have raised widespread interest of multi-view clustering, in particular, the deep multi-view clustering, which is the main purpose of this paper.

The existing deep multi-view learning approaches generally perform clustering in a separated manner, *i.e.*, extracting multi-view representations based on deep architectures, then conducting traditional clustering such as K-means or spectral clustering. Andrew et al. (G. Andrew and Livescu 2013) proposed deep canonical correlation analysis (DCCA) to learn complex nonlinear transformations for each of the two views, such that the resulting representations are highly linearly correlated. The deep canonically correlated autoencoders (DCCAE) (W. Wang and Bilmes 2015) improved the DCCA by adding a reconstruction loss into whole objective function. To overcome the limitation of handling only two views, Benton et al. (A. Benton 2017) proposed the deep generalized canonical correlation analysis (DGCCA), which simultaneously learned nonlinear mappings and a shared representation from data with more than two views. While these approaches can obtain promising multi-view representations, such a kind of two-stage learning strategy usually brings some limitations (G. Chao and Bi 2018).

To pursue better clustering performance, several deep jointly learning methods (J. Xie and Farhadi 2016; J. Yang and Batra 2016) have been proposed. Among them, the most representative work is the deep embedded clustering (DEC) (J. Xie and Farhadi 2016), which is inspired by the parametric t-SNE (van der Maaten 2009), defining a centroid-based soft assignment distribution and minimizing its Kullback-Leibler (KL) divergence to an auxiliary target distribution to jointly learn feature representation and clustering assignment. Nevertheless, existing jointly deep clustering models mainly belong to the single-view method, leading to the loss of complementary information from multiple heterogeneous feature spaces.

How to integrate multi-view learning and deep jointly clustering is no doubt challenging. In this paper, we propose a novel deep multi-view clustering model by jointly learning multiple deep embedding features, multi-view weighting scheme, and clustering assignment in a unified deep architecture. Taking inspiration from the DEC and multiple embedding t-SNE (B. Xie and Huang 2011), we employ a KL divergence to match the centroid-based soft assignment to a *multi-view fused target distribution*, which can lead to more refined clustering predictions. We refer to this model as Deep Multi-View Clustering via Multiple Embedding (DMVC-ME). Fig. 1 illustrates the flowchart of the

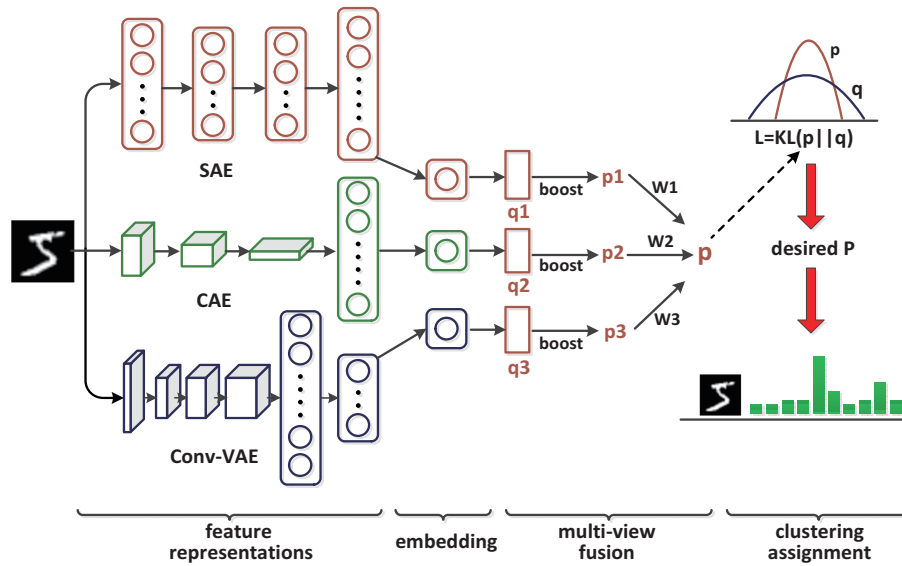


Figure 1: The flowchart of the proposed DMVC-ME on grayscale image datasets. (1) feature representations: there are two techniques to construct multi-view branches, *i.e.*, feeding the same input into different network architectures or feeding distinct inputs into the same network architecture. (2) embedding: the features are extracted from the embedding layers of multi-view branches to feed into the next part. (3) multi-view fusion: a multi-view fused target distribution \mathbf{p} is introduced to refine the view-specific soft assignment based on the KL divergence. (4) clustering assignment: the multi-view fused target distribution \mathbf{p} is used to predict right clusters, *i.e.*, each sample is assigned to the cluster with the highest prediction probability.

proposed model. Our component of deep feature representations is based on various kinds of autoencoders, each of which is regarded as one view (branch)* (see the feature representations part in Fig. 1). The parameters of DMVC-ME are updated by an alternating optimization scheme. Besides the pretraining of deep branches, our model can be efficiently optimized in an end-to-end manner. To the best of our knowledge, there are hardly any deep multi-view clustering models, in particular, the ones with joint learning strategy as well as end-to-end training. We summarize our major contributions as follows:

- We propose a new type of deep multi-view clustering framework to jointly learn multiple feature representations, multi-view fusion mechanism, and clustering assignment in an integrated deep framework. Specifically, the multi-view constraint is imposed on the auxiliary target distribution, which can effectively take advantage of the complementary traits of multiple views and guides clustering more accurately. Moreover, the proposed model can be trained in an end-to-end way.
- To study the performance of the proposed model, extensive experiments and evaluation are conducted on several challenging image datasets, including grayscale image datasets and three-channel image datasets. A significant improvement can be observed over single/multi-view baselines and the state-of-the-art multi-view clustering methods, which demonstrates the effectiveness of the proposed model.

*For ease of understanding, we do not distinguish between view and branch.

Related Work

Before introducing the proposed model, we give a brief review of the recent progress on the two topics most related with it, *i.e.*, multi-view clustering and deep clustering.

Multi-View Clustering. Multi-view clustering can be roughly divided into discriminative approaches and generative approaches. Among them, the former attracts much more attention, and can be further divided into three categories according to (G. Chao and Bi 2018): (1) direct view combination; (2) common structure based methods; (3) view combination after projection. We mainly focus on the last two categories in this paper. For common structure based methods, one general idea is to enforce a common indicator matrix by using the nonnegative matrix factorization (NMF) among different views. Cai *et al.* (X. Cai and Huang 2013) proposed a multi-view k-means clustering method (RMKMC) by introducing a common indicator matrix across different views, which can adapt to large scale datasets. The multi-view self-paced clustering (MSPL) (C. Xu 2015), which is an improvement of RMKMC, learned the multi-view model by taking the complexities of the samples and views into account. The representative methods for the last category are proposed in (Blaschko and Lampert 2008; K. Chaudhuri and Sridharan 2009), which applied canonical correlation analysis (CCA) and kernel CCA to project the multi-view high-dimensional data onto a low-dimensional subspace, respectively.

Deep clustering. Traditional deep clustering methods usually performs clustering separately, *i.e.*, it first trains a deep feature extractor, and then applies a clustering algorithm (K-means or spectral clustering) to the extracted features (X. Peng 2016; F. Tian 2014; P. Huang and Wang 2014). However, the learned deep feature might be suboptimal for clustering due to the separated process. Recently, clustering methods, which jointly learn feature representations and clustering assignments using deep networks (J. Xie and Farhadi 2016; J. Yang and Batra 2016; B. Yang and Hong 2017), have been proposed. Deep clustering network (DCN) (B. Yang and Hong 2017) proposed a joint dimensional reduction and k-means clustering framework, where the dimensional reduction model is based on deep neural networks. Motivated by the t-SNE (van der Maaten 2009), the deep embedded clustering (DEC) (J. Xie and Farhadi 2016) employed a deep stacked autoencoder (SAE) (P. Vincent and Manzagol 2010) to initialize the feature extraction model, and then iteratively optimized a KL divergence based clustering objective with a self-training target distribution.

The joint learning methods have shown great superiority beyond the separated ones. However, most joint learning methods concentrate on single-view framework, ignoring the complementary information from multiple heterogeneous views. The proposed model, different from aforementioned methods, learns multiple feature representations, multi-view fusion mechanism, and clustering assignment in a unified framework, which can achieve promising clustering performance and accommodate well on large scale datasets.

The Proposed Method

Consider the problem of clustering a set of n data points into k clusters by using multi-view features $\{\mathbf{x}_i^{(v)} \in \mathbf{X}^{(v)}\}_{i=1}^n$, where the $\mathbf{X}^{(v)}$ denotes the original v -th feature space, and each cluster is represented by a centroid $\boldsymbol{\mu}_j^{(v)}, j = 1, \dots, k$. Instead of conducting multi-view clustering directly in the original feature spaces $\{\mathbf{X}^{(v)}\}_{i=1}^n$, we aim to first transform the original features with non-linear mapping $f_{\boldsymbol{\theta}^{(v)}}^{(v)} : \mathbf{X}^{(v)} \rightarrow \mathbf{Z}^{(v)} (v = 1, \dots, V)$, where $\boldsymbol{\theta}^{(v)}$ represents the learnable hyperparameters of mapping functions for the v -th view, $\mathbf{Z}^{(v)}$ is the latent *embedded feature space*. Note that $\{\mathbf{X}^{(v)}\}_{i=1}^n$ are unnecessary to be distinctive, since we can employ different deep architectures to the same feature, *e.g.*, use SAE and CAE on raw image pixels, to obtain different non-linear features in embedded feature spaces.

The proposed algorithm clusters data by simultaneously learning view-specific k cluster centers $\{\boldsymbol{\mu}_j^{(v)}\}_{j=1}^k$ in the embedded feature space $\mathbf{Z}^{(v)}$, the parameters $\boldsymbol{\theta}^{(v)}$ of the deep network that maps original feature in $\mathbf{X}^{(v)}$ into $\mathbf{Z}^{(v)}$, and the multi-view fusion parameters in a unified way. It has two phases: (1) parameters initialization with multiple deep architectures; (2) the alternative optimization of view-specific cluster centers, network weight parameters, and multi-view fusion parameters. We elaborate our proposed method and the optimization scheme in the following.

Problem Formulation

Following the DEC (J. Xie and Farhadi 2016), when given the initial estimation of non-linear mappings $f_{\boldsymbol{\theta}^{(v)}}^{(v)}$ and the initial cluster centroids $\{\boldsymbol{\mu}_j^{(v)}\}_{j=1}^k$, we adopt the Student's t -distribution as the soft assignment to measure the similarity between the embedded feature $\mathbf{z}_i^{(v)}$ and the cluster center $\boldsymbol{\mu}_j^{(v)}$:

$$\mathbf{q}_{ij}^{(v)} = \frac{(1 + \|\mathbf{z}_i^{(v)} - \boldsymbol{\mu}_j^{(v)}\|^2/\alpha)^{-\frac{\alpha+1}{2}}}{\sum_{j'} (1 + \|\mathbf{z}_i^{(v)} - \boldsymbol{\mu}_{j'}^{(v)}\|^2/\alpha)^{-\frac{\alpha+1}{2}}}, \quad (1)$$

where $\mathbf{z}_i^{(v)} = f_{\boldsymbol{\theta}^{(v)}}^{(v)}(\mathbf{x}_i^{(v)}) \in \mathbf{Z}^{(v)}$ corresponds to $\mathbf{x}_i^{(v)}$ by non-linear embedding, α represents the degree of freedom of the Student's t -distribution. $\mathbf{q}_{ij}^{(v)}$ is referred to as the *soft assignment* because it can be interpreted as the probability of assigning sample i to cluster j in the v -th view.

In DEC, the clusters are iteratively refined resorting to a powerful auxiliary target distribution, which is defined as

$$\mathbf{p}_{ij}^{(v)} = \left(\mathbf{q}_{ij}^{(v)}\right)^\gamma, \gamma > 1, \text{ s.t. } \sum_j \mathbf{p}_{ij}^{(v)} = 1. \quad (2)$$

This target distribution can guide clustering by learning from high confidence assignments. In all experiments, we simply set $\alpha = 1$ and $\gamma = 2$.

To realize multi-view fusion, we introduce multi-view combination coefficients, which will be imposed on the final target distribution:

$$\mathbf{p}_{ij} = \sum_{v=1}^V \mathbf{w}_v \mathbf{p}_{ij}^{(v)}, \quad (3)$$

where \mathbf{w}_v is the nonnegative weight for the v -th view, with the strong constraints that $\mathbf{w}_v > 0$ and $\sum_v \mathbf{w}_v = 1$. This *multi-view target distribution* is a linear combination of all the view-specific target distribution, which serves as a more powerful instruction for view-specific soft assignment distribution. The final objective function is defined as:

$$\begin{aligned} \mathcal{L}(\boldsymbol{\mu}_j^{(v)}, \boldsymbol{\theta}^{(v)}, \mathbf{w}) = & \min_{\boldsymbol{\mu}_j^{(v)}, \boldsymbol{\theta}^{(v)}, \mathbf{w}} \sum_{v'} \sum_i \sum_j \left\{ \sum_{v=1}^V \mathbf{w}_v \mathbf{p}_{ij}^{(v)} \log \frac{\sum_{v=1}^V \mathbf{w}_v \mathbf{p}_{ij}^{(v)}}{\mathbf{q}_{ij}^{(v')}} \right\} + \lambda \|\mathbf{w}\|^2, \\ \text{s.t. } & \mathbf{w}_v > 0, \sum_v \mathbf{w}_v = 1. \end{aligned} \quad (4)$$

Note that the second term, *i.e.*, l_2 -norm of \mathbf{w} , is introduced as a regularization term to avoid the trivial solution (*e.g.*, only one of \mathbf{w}_v is equal to 1), which means that only one view works, while the contributions of the other views vanish. The parameter λ is used to balance the effect of the two parts in (4).

Optimization Procedure

In the initialization stage, each branch is pretrained to extract deep embedded features by using the reconstruction

Algorithm 1: Deep Multi-View Clustering via Multiple Embedding

Input: $\{\mathbf{X}^{(v)}\}_{v=1}^V, E, B, m_b, \gamma$ and cluster number K
Output: hard assignments \mathcal{C}

// —Stage 1: Initialization of multi-view networks and view-specific cluster centers

```

1 for  $v = 1 : V$  do
2   | Pretrain the  $v$ -th deep branch;
3 end
   Initialize  $\mathbf{w}_v = 1/V$  ( $v = 1, \dots, V$ );
   Forward propagate  $v$ -th network to get  $\mathbf{z}_i^{(v)}$  and use
   K-means to obtain initial cluster centers
    $\{\mu_1^{(v)}, \dots, \mu_K^{(v)}\}_{v=1}^V$ ;
// —Stage 2: Optimization of DMVC-ME
4 for  $e = 1 : E$  do
   // Fix  $\mathbf{w}$  to optimize  $\mu_i^{(v)}$  and  $\theta^{(v)}$ 
5   for  $v = 1 : V$  do
6     for  $b = 1 : B$  do
7       | Forward propagate  $v$ -th network with a
7       | mini-batch of  $m_b$  samples in  $\mathbf{X}^{(v)}$ ;
8       | Backward propagate  $v$ -th network to get
8       |  $\partial \mathcal{L} / \partial \theta^{(v)}$  and  $\partial \mathcal{L} / \partial \mu^{(v)}$ ;
9       | Update  $\theta^{(v)}$  and  $\mu^{(v)}$  with the gradients;
10    end
11  end
   // Fix  $\mu_i^{(v)}$  and  $\theta^{(v)}$  to optimize  $\mathbf{w}$ 
12  for  $v = 1 : V$  do
13    | Calculate  $\mathbf{z}_i^{(v)}$  by using updated  $\theta^{(v)}$ ;
14    | Update  $\mathbf{q}_{ij}^{(v)}$  and  $\mathbf{p}_{ij}^{(v)}$  by using (1) and (2),
14    | respectively;
15  end
16  Calculate multi-view target distribution  $\mathbf{p}_{ij}$  by
16  using (3);
17  Obtain combination weight  $\mathbf{w}$  by solving (7);
18  Stop if hard assignments change  $\leq$  tolerance.
19 end
20 return hard assignments  $\mathcal{C}$ 

```

loss. Then the optimization is over network parameters $\theta^{(v)}$, view-specific cluster centers $\mu_i^{(v)}$, and multi-view weight \mathbf{w} . We adopt alternative optimization to solve this problem. Specifically, in every iteration, we fix \mathbf{w} to use KL divergence to update $\mu_i^{(v)}$ and $\theta^{(v)}$. After that, we fix $\mu_i^{(v)}$ and $\theta^{(v)}$ to optimize \mathbf{w} . The initial value of \mathbf{w}_v is set as $\mathbf{w}_v = 1/V$, with V representing the number of views. The details of optimization procedure are given below:

Optimize $\mu_i^{(v)}$ and $\theta^{(v)}$ by fixing \mathbf{w} : since \mathbf{w} is fixed, for the v -th view, the objective function \mathcal{L} is reduced to a KL divergence. The cluster center $\mu_i^{(v)}$ and hyperparameter $\theta^{(v)}$ can be jointly optimized by using Stochastic Gradient Descent (SGD) with momentum. It is worth noting that, the

target distribution and soft assignment distribution need not be updated synchronously, so the $\mathbf{p}_{ij}^{(v)}$ can be considered to be independent of $\mu_j^{(v)}$ and $\theta^{(v)}$ in practice.

The gradients of \mathcal{L} w.r.t embedded feature $\mathbf{z}_i^{(v)}$ and each cluster center $\mu^{(v)}$ can be calculated as:

$$\frac{\partial \mathcal{L}}{\partial \mathbf{z}_i^{(v)}} = \frac{\alpha + 1}{\alpha} \sum_j \left(1 + \frac{\|\mathbf{z}_i^{(v)} - \mu_j^{(v)}\|^2}{\alpha} \right)^{-1} (\mathbf{p}_{ij} - \mathbf{q}_{ij}^{(v)}) (\mathbf{z}_i^{(v)} - \mu_j^{(v)}), \quad (5)$$

$$\frac{\partial \mathcal{L}}{\partial \mu_j^{(v)}} = -\frac{\alpha + 1}{\alpha} \sum_i \left(1 + \frac{\|\mathbf{z}_i^{(v)} - \mu_j^{(v)}\|^2}{\alpha} \right)^{-1} (\mathbf{p}_{ij} - \mathbf{q}_{ij}^{(v)}) (\mathbf{z}_i^{(v)} - \mu_j^{(v)}). \quad (6)$$

Then, the gradients of the hyperparameters of the v -th deep network, i.e., $\partial \mathcal{L} / \partial \theta^{(v)}$, can be calculated by using the standard backpropagation with the input $\partial \mathcal{L} / \partial \mathbf{z}_i^{(v)}$.

Optimize \mathbf{w} by fixing $\mu_i^{(v)}$ and $\theta^{(v)}$: since $\mathbf{p}_{ij}^{(v)}$ and $\mathbf{q}_{ij}^{(v)}$ are fixed, the objective function w.r.t \mathbf{w} is formulated as:

$$\begin{aligned} \mathcal{L}(\mathbf{w}) &= \min_{\mathbf{w}} \sum_{v'} \sum_i \sum_j \mathbf{p}_{ij} \log \frac{\mathbf{p}_{ij}}{\mathbf{q}_{ij}^{(v')}} + \lambda \|\mathbf{w}\|^2, \\ \text{s.t. } \mathbf{w}_v &> 0, \quad \sum_v \mathbf{w}_v = 1. \end{aligned} \quad (7)$$

Proposition 1. *The objective function $\mathcal{L}(\mathbf{w})$ is convex.*

It can be easily proved: the KL divergence is convex w.r.t \mathbf{p}_{ij} , which is linear with \mathbf{w} . Moreover, the l_2 -norm is a convex function of \mathbf{w} . Therefore, the $\mathcal{L}(\mathbf{w})$ is convex w.r.t \mathbf{w} . This subproblem can be efficiently solved by accelerated proximal gradient (APG) method (Beck and Teboulle 2009).

Once all the parameters have been optimized, the predicted label for the unlabeled data can be calculated by the following function:

$$\mathbf{y}_i = \operatorname{argmax}_j \mathbf{p}_{ij}. \quad (8)$$

Finally, the optimization procedure of the objective function (4) is summarized in Algorithm 1, where E is the maximum learning epochs, B is the number of batches in each epoch and m_b is the batch size.

Experimental Results and Analysis

We evaluate the proposed DMVC-ME on several popular image datasets with three most frequently used clustering measures. Moreover, we investigate the performance of our model via a series of ablation studies. All experiments are implemented on a workstation with Intel (R) Core (TM) i7-7700K @ 4.20GHz CPU, 120GB RAM, and GeForce GTX 1080 GPU (8GB caches). The source codes and experimental results will be released at <https://github.com/expectorlin/DMVC>.

Experimental Setting

Datasets We perform experiments on five popular image datasets, including MNIST (Y. LeCun and P.Haffner 1998), fashion-MNIST (Han Xiao 2017), USPS (Hull 1994), STL-10 (A. Coates and Lee 2011), and CIFAR-10 (Krizhevsky and Hinton 2009). **MNIST** consists of 70K grayscale handwritten digit images with a size of 28×28 pixels from 10 categories. **fashion-MNIST** contains 70K fashion product images from 10 classes, with the same image size to MNIST. **USPS** includes 9298 grayscale handwritten digits with the size of 16×16 from 10 categories. **STL-10** incorporates 13K three-channel images with the size of 96×96 pixels from 10 different object classes. **CIFAR-10** is similar to STL-10, which comprises 60K three-channel images of 10 object categories. The image size in CIFAR-10 is 32×32 pixels. The statistics of all the datasets are summarized in Table 1. Note that the training and testing images of each dataset are jointly utilized for clustering.

Table 1: The summary of data statistics.

Datasets	Images	Classes	Image sizes
MNIST	70000	10	(28,28,1)
fashion-MNIST	70000	10	(28,28,1)
USPS	9298	10	(16,16,1)
STL-10	13000	10	(96,96,3)
CIFAR-10	60000	10	(32,32,3)

Network Configurations We employ the stacked autoencoder (SAE) (P. Vincent and Manzagol 2010), convolutional variational autoencoder (Conv-VAE) (T. Kulkarni and Tenenbaum 2015), and convolutional autoencoder (CAE) (Guo X 2017) as three single-view deep network branches for gray-scaled image datasets MNIST, fashion-MNIST and USPS. For Conv-VAE and CAE, the original image is taken as the network input. Since the layers of SAE are densely connected, the raw image is converted into a long vector to feed into the input layer.

For three-channel image datasets *i.e.*, STL-10 and CIFAR10, we use two SAE networks with different input features and one variational autoencoder (VAE) network as the single-view deep network branches. To pursue better performance, we employ deep features as the input of different views. Specifically, the deep features are extracted from the fully-connected layers of three powerful networks, *i.e.*, the VGG-16 (Simonyan and Zisserman 2014), ResNet50 (K. He and Sun 2016), and Inception-V3 (C. Szegedy and Wojna 2015), all of which are pre-trained on ILSVRC12 (J. Deng and Fei-Fei 2009). A detailed configurations of the single-view deep network branches in our model, the corresponding network architectures and the network inputs on different datasets are given in Table 2.

Compared Methods We compare the proposed DMVC-ME with one multi-view baseline, the corresponding single-view baselines, and several state-of-the-art multi-view clustering approaches. For the single-view competitors, we consider their learning strategies in two different ways. Similar

Table 2: The detailed configurations of the proposed model on different datasets.

Datasets	Network Branch	Architecture	Network input
MNIST fashion-MNIST USPS	SAE(View1)	500-500-2000-10	vectorized raw image
	Conv-VAE(View2)	conv1($2 \times 2 \times 1$)-conv2($2 \times 2 \times 6$)-conv3($3 \times 3 \times 20$)-conv4($3 \times 3 \times 60$)-flatten-256-10	raw image pixels
	CAE(View3)	conv1($5 \times 5 \times 32$, strides=2)-conv2($5 \times 5 \times 64$, strides=2)-conv3($3 \times 3 \times 128$, strides=2)-flatten-10	raw image pixels
STL-10 CIFAR-10	SAE(View1)	500-500-2000-10	VGG16 feature
	SAE(View2)	500-500-2000-10	ResNet50 feature
	VAE(View3)	500-256-50	Inception-V3 feature

to DEC (J. Xie and Farhadi 2016), the first strategy is jointly learning feature representations and clustering assignments, which is referred to as **J-View-i**, where i denotes the i -th deep network branch in our model. The other way (denoted as **S-View-i**) performs clustering disjointedly: it first trains the single deep autoencoder by using the reconstruction loss, then performs K-means based on the extracted embedding feature. As for the multi-view baseline (named as **All-Views**), we pretrain all the deep branches in our model independently, and then concatenate all the embedding features directly to perform K-means.

Moreover, several representative multi-view clustering algorithms are also compared with our model, including DCCA (G. Andrew and Livescu 2013), DCCAE (W. Wang and Bilmes 2015), DGCCA (A. Benton 2017), RMKMC (X. Cai and Huang 2013) and MSPL (C. Xu 2015). The first three methods belong to DNN-based multi-view approaches, while the last two are the traditional multi-view clustering methods designing for large-scale dataset.

Evaluation Metrics To measure the clustering performance of different algorithms, we adopt three standard clustering measures, *i.e.*, clustering accuracy (ACC), Normalized Mutual Information (NMI) and Adjusted Rand Index (ARI). These measures range in $[0, 1]$, and for each of the metrics, the higher it is, the better the performance is. All the evaluation metrics adopted in our manuscript belong to external criteria (M. Christopher D. and Schtze 2010).

Implementation Details For DMVC-ME, we apply the Adam optimizer (Kingma and Ba 2015) in the pretraining process for all the deep views and the Adagrad optimizer (J. Duchi and Singer 2011) in the joint optimization process. The batch size for pretraining and joint optimization is set to 256, and the tolerance for convergence is set to 0.0001 (step 18 in Algorithm 1). The maximum numbers of training epochs in the optimization process are set to 100 and 2000 for grayscale image datasets and three-channel image datasets, respectively. The balance factor λ is set as 2.0×10^4 for all datasets.

To make a fair comparison, for each dataset, we set the

Table 3: The clustering results on MNIST, fashion-MNIST, USPS, STL10 and CIFAR10.

Method	MNIST			fashion-MNIST			USPS			STL10			CIFAR10		
	ACC	NMI	ARI	ACC	NMI	ARI	ACC	NMI	ARI	ACC	NMI	ARI	ACC	NMI	ARI
RMKMC	0.8255	0.7995	0.7524	0.5912	0.6169	0.4636	0.7441	0.7278	0.6667	0.8344	0.8273	0.7635	0.5714	0.4688	0.3679
MSPL	0.8717	0.8147	0.7892	0.5607	0.6068	0.4457	0.7414	0.7174	0.6370	0.8108	0.8220	0.7402	0.7156	0.5948	0.5174
DCCA	0.3155	0.2086	0.1272	0.4105	0.4028	0.2342	0.4042	0.3895	0.2480	0.8411	0.7477	0.6917	0.4242	0.3385	0.2181
DCAE	0.3029	0.2038	0.1274	0.4109	0.3836	0.2303	0.3793	0.3246	0.2135	0.8235	0.7273	0.6632	0.3960	0.3226	0.2034
DGCCA	0.4714	0.3840	0.2789	0.4765	0.4827	0.3105	0.5473	0.5079	0.4011	0.8960	0.8218	0.7970	0.4703	0.3577	0.2634
S-View-1	0.8901	0.8229	0.8034	0.5855	0.6240	0.4610	0.7357	0.7195	0.6363	0.8169	0.7415	0.6617	0.2983	0.1772	0.1024
S-View-2	0.7971	0.6979	0.6545	0.5443	0.5044	0.3721	0.6696	0.6479	0.5716	0.8327	0.7562	0.6914	0.4331	0.3359	0.2243
S-View-3	0.8888	0.8068	0.7888	0.5793	0.6343	0.4632	0.7062	0.6842	0.5813	0.8224	0.7305	0.6411	0.7162	0.5714	0.5013
All-Views	0.9062	0.8286	0.8181	0.5993	0.6348	0.4756	0.7367	0.7231	0.6420	0.9298	0.8674	0.8525	0.7552	0.6069	0.5428
J-View-1	0.9378	0.9123	0.9018	0.5982	0.6407	0.4820	0.7831	0.8170	0.7435	0.8372	0.7570	0.7038	0.3035	0.1832	0.1094
J-View-2	0.8929	0.8644	0.8236	0.5886	0.6011	0.4434	0.7465	0.7864	0.6973	0.8466	0.7658	0.7145	0.4423	0.3447	0.2398
J-View-3	0.9071	0.8251	0.8208	0.5462	0.5841	0.4136	0.7610	0.7602	0.6888	0.8939	0.8212	0.7863	0.7613	0.6424	0.5721
DMVC-ME	0.9603	0.9312	0.9316	0.6087	0.6442	0.4864	0.7865	0.8222	0.7480	0.9471	0.8919	0.8872	0.7954	0.6784	0.6291

same configurations, including optimizers, initializers, and batch sizes for the proposed model and the **J-View-i** algorithms. Moreover, the initialized network parameters of **J-View-i** are kept the same as our model. We also use the pre-trained network weights in our model to extract features for **S-View-i**, **All-Views**, **RMKMC** and **MSPL**.

Since DCCA and DCAE can only deal with two views, we choose the best two views in our model according to their performance as the two branches. After optimization, we concatenate the embedding features in two branches to perform K-means. Besides, the balance factor between reconstruction loss and the CCA loss (W. Wang and Bilmes 2015) in DCAE is set to 0.5 for all datasets. For DGCCA, we use the shared representations to perform K-means directly. The initialized network weights of DCCA, DCAE and DGCCA are also kept consistent with our model.

Experimental results In this subsection, we report the quantitative results of different clustering methods. For each method, we run the experiments for 10 times on each dataset and get the average results. The results on five image datasets are shown in Table 3. Note that our model DMVC-ME significantly outperforms other clustering algorithms with all the metrics on both gray-scaled image datasets and three-channel image datasets. We can observe that on all datasets, the clustering performance of DMVC-ME will not be affected by the worst branch and what is more, they can achieve considerably higher accuracy than the best branch. The experiment results demonstrate that combining the joint learning framework and multi-view clustering is feasible and effective. Furthermore, we can also find that end-to-end clustering methods are superior to the separated ones obviously, which shows the importance of joint learning.

Ablation Studies

Contributions of Multi-View Networks Since DMVC-ME is based on joint optimizing framework, we investigate the effectiveness of multi-view joint learning and the impact of different views on our model. To do the former, we report the change of the clustering accuracy (ACC) in the optimization process, as illustrated in Fig. 2, where the ACC results of DMVC-ME could be boosted during the optimization process on both STL-10 and CIFAR-10. Note that sim-

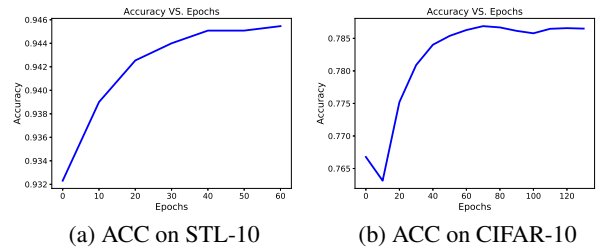
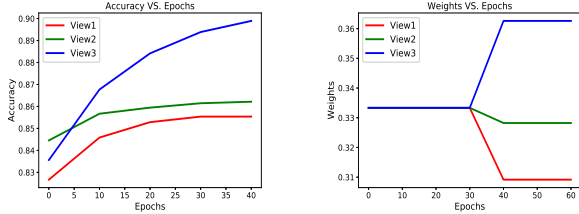


Figure 2: The accuracy increment during the optimization process of DMVC-ME on STL-10 and CIFAR-10.

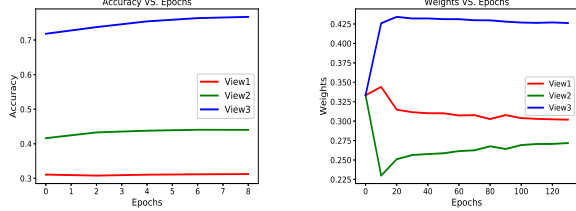
ilar observations can be obtained from other datasets. The apparent performance gain proves that jointly learning multiple feature representations, multi-view fusion, and clustering assignment in a unified deep architecture can effectively capture the relationship among large scale unlabeled data.

To do the latter, we show the variation of the multi-view weights, as well as the change of the ACC results of different views during the optimization process on STL-10 and CIFAR-10. The related results are presented in Fig. 3, where we can obviously find the view-specific boost from all the branches, which supports the overall performance gain of DMVC-ME. Furthermore, the order of color curves indicates that, the best view (the VAE branch with Inception-V3 feature in Table 2, the blue curve in Fig. 3 (a) and (c)) will dominate the final result in the learning process (the blue curve in Fig. 3 (b) and (d)), while other views can not be ranked according to their individual performance. Probably this is due to the importance degree of complementary information in specific view.

Sensitivity for Initialization The joint learning framework usually contains the initialization stage and the optimization stage. Investigating the sensitivity for initialization can ensure whether or not the proposed model can achieve stable performance in most cases. Therefore, we report the variance of the ACC for both DMVC-ME and **J-View-i** on two grayscale image datasets (fashion-MNIST and USPS) and two three-channel image datasets (STL-10 and CIFAR-



(a) View-specific ACC on STL-10 (b) Weights variation on STL-10



(c) View-specific ACC on CIFAR-10 (d) Weights variation on CIFAR-10

Figure 3: The accuracy increment and weights variation of all the views for DMVC-ME on STL-10 and CIFAR-10.

Table 4: The variance of ACC on fashion-MNIST, USPS, STL-10 and CIFAR-10.

Method	fashion-MNIST	USPS	STL10	CIFAR10
J-View-1(CAE)	0.001753	6.29e-5	0.001977	0.000225
J-View-2(Conv-VAE)	0.000689	0.001697	0.001672	0.000163
J-View-3(SAE)	0.001628	4.24e-5	0.000241	0.001481
DMVC-ME	0.000929	3.11e-5	1.20e-6	4.66e-5

10). For all these datasets, we run all the methods for 50 times to obtain the variance, which are given in Table 4. We can find that relatively low variance is kept by DMVC-ME, indicating the good stability of the proposed model.

Robustness for Integrating Different Views In the aforementioned experiments, we fix the number of views (usually three) in DMVC-ME. To study the impact of number of views on our model, we construct the proposed model with two, three, and four network branches, where the configurations are (Conv-VAE + SAE), (CAE + Conv-VAE + SAE), and (CAE + Conv-VAE + SAE + VAE), respectively. For limited space, we only report the related clustering results of our model and corresponding single-view baseline algorithms **J-View-*i*** on MNIST, which are shown in Table 5.

Compared with the J-View-2 and J-View-3, the two-view DMVC-ME achieve better performances (93.88% vs 89.29% and 90.71% in terms of ACC), which indicates that two types of features generated by the Conv-VAE and SAE can complement each other well. Moreover, compared with three-view counterpart, the two-view model can still achieve highly competitive result even through a good branch, *i.e.*, CAE, has been removed. Furthermore, when adding a *de-generative view* (VAE, the ACC of J-View-4 is 70.59%) into

our three-view model, the effect on clustering performance is limited with a reasonable margin (88.28%). These experimental results sufficiently demonstrate that the proposed DMVC-ME exhibits robustness for incorporating different views.

Table 5: The clustering results of DMVC-ME with incorporating different types of views on MNIST.

Methods	ACC	NMI	ARI
J-View-1 (CAE)	0.9378	0.9123	0.9018
J-View-2 (Conv-VAE)	0.8929	0.8644	0.8236
J-View-3 (SAE)	0.9071	0.8251	0.8208
J-View-4 (VAE)	0.7059	0.6930	0.5769
DMVC-ME (Conv-VAE + SAE)	0.9388	0.9090	0.8993
DMVC-ME (CAE + Conv-VAE + SAE)	0.9603	0.9312	0.9316
DMVC-ME (CAE + Conv-VAE + SAE + VAE)	0.8828	0.8702	0.8370

Optimal Number of Clusters In the previous subsection, we have assumed that the number of clusters on each dataset is predefined according to its groundtruth. However, in the real applications, this number is usually unknown. Here, similar to DEC (J. Xie and Farhadi 2016), we run the proposed DMVC-ME on MNIST with different number of clusters as input to find its optimum, whose quality is measured by the Normalized Mutual Information (NMI). Fig. 4 shows the detailed NMI results, where we can find that our DMVC-ME achieve highest NMI at the number of 10 (equal to the groundtruth), which demonstrates that our method holds a well capability of uncovering the underlying data distribution. This result is superior to that of DEC, which confuses the number 9 and 4 such that it tends to segment all the hand-written digit into 9 clusters.

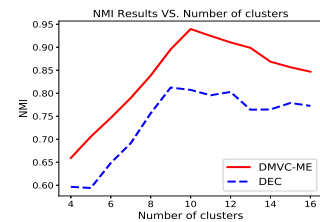


Figure 4: The NMI results of DMVC-ME with different number of clusters on MNIST.

Conclusions

In this study, we proposed a novel deep multi-view clustering model that can learn deep embedded features, multiple weighting mechanism and clustering assignment concurrently. Specifically, the KL divergence loss is minimized between the centroid-based soft assignment distribution and an auxiliary multi-view fused target distribution. In this way, the complementary information among multiple views can be well exploited to guide clustering. Moreover, the learned multi-view features are more clustering-friendly. The experimental results on both grayscale and three-channel image

datasets fully substantiate the effectiveness and robustness of our proposed model.

Appendix

To further demonstrate the performance of the proposed model, we present the whole experimental results of our study in this section. Specifically, we first introduce all the image datasets we tested, then the network configurations of our proposed model on all datasets will be given. Finally, we report the complete experiment results on all the datasets.

Datasets

We evaluate the proposed DMVC-ME on eight popular image datasets totally, including four grayscale image datasets: MNIST (Y. LeCun and P.Haffner 1998), fashion-MNIST (Han Xiao 2017), USPS (Hull 1994) and COIL-20 (F. Li and Xi 2018), and four three-channel image datasets: STL-10 (A. Coates and Lee 2011), CIFAR-10 (Krizhevsky and Hinton 2009), CIFAR-100 (Krizhevsky and Hinton 2009) and SUN-397 (Xiao J 2010). **MNIST** includes 70K grayscale hand-written digit images with a size of 28×28 pixels from 10 categories. **fashion-MNIST** is a collection of fashion products, consisting of 70K 28×28 grayscale images of 10 classes. **USPS** dataset comprises 9298 grayscale hand-written digits with the size of 16×16 from 10 categories. **COIL-20** dataset collects 1440 128×128 grayscale object images of 20 categories viewed from varying angles, with each category including 72 images. We resize the image size to 32×32 pixels. **STL-10** contains 13K three-channel object images with the size of 96×96 pixels from 10 categories. **CIFAR-10** dataset is similar to STL-10, which incorporates 60K three-channel images of 10 object categories. The image size in CIFAR-10 is 32×32 pixels, which is significantly lower than that in STL-10. **CIFAR-100** dataset shares the same number of images with CIFAR-10 but with 100 object categories, and each class contains 600 images. **SUN-397** dataset includes 108,754 scene images from 397 categories. The number of images varies across categories, with at least 100 images per category. It is a extremely challenging dataset for clustering methods. We summarize the statistics of all the datasets in Table 6.

Table 6: The summary of data statistics.

Datasets	Images	Classes	Image sizes
MNIST	70000	10	(28,28,1)
fashion-MNIST	70000	10	(28,28,1)
USPS	9298	10	(16,16,1)
COIL-20	1440	20	(32,32,1)
STL-10	13000	10	(96,96,3)
CIFAR-10	60000	10	(32,32,3)
CIFAR-100	60000	100	(32,32,3)
SUN-397	108754	397	\

Network Configurations

For four grayscale image datasets MNIST, fashion-MNIST, USPS and COIL-20, we employ SAE, conv-VAE and CAE

as three single-view deep branches in our model. For conv-VAE and CAE, we feed the raw image into the input layer. For SAE, the raw image is pulled into a long vector as the input. For four three-channel image datasets STL-10, CIFAR-10, CIFAR-100 and SUN-397, we use two SAE networks with different inputs and a VAE network as the single-view deep branches in our model. To achieve better performance, we extract deep features from four powerful networks, *i.e.*, the AlexNet (A. Krizhevsky and Hinton 2012), VGG-VD (Simonyan and Zisserman 2014), ResNet50 (K. He and Sun 2016), and Inception-V3 (C. Szegedy and Wojna 2015), as the input of single-view branches. All of these networks are pre-trained on ILSVRC12 (J. Deng and Fei-Fei 2009). The detailed configurations of the single-view deep network branches in our model, the corresponding network architectures and the network inputs on different datasets are given in Table 7.

Table 7: The detailed configurations of the proposed model on different datasets.

Datasets	Network Branch	Architecture	Network input
MNIST fashion-MNIST USPS COIL-20	SAE(View1)	500-500-2000-10	vectorized raw image
	Conv-VAE(View2)	conv1($2 \times 2 \times 1$)-conv2($2 \times 2 \times 6$)-conv3($3 \times 3 \times 20$)-conv4($3 \times 3 \times 60$)-flatten-256-10	raw image pixels
	CAE(View3)	conv1($5 \times 5 \times 32$, strides=2)-conv2($5 \times 5 \times 64$, strides=2)-conv3($3 \times 3 \times 128$, strides=2)-flatten-10	raw image pixels
STL-10 CIFAR-10 CIFAR-100	SAE(View1)	500-500-2000-10	VGG16 feature
	SAE(View2)	500-500-2000-10	ResNet50 feature
	VAE(View3)	500-256-50	Inception-V3 feature
SUN397	SAE(View1)	2000-500-50-10	Alexnet feature
	SAE(View2)	2000-500-50-10	Inception-V3 feature
	VAE(View3)	2000-256-10	VGG19 feature

Experimental results

To show the experimental results more clearly, we divide the results into two groups and present them in Table 8 and Table 9 respectively. Specifically, The results on four grayscale image datasets MNIST, fashion-MNIST, USPS and COIL-20 are shown in Table 8 and the results on four three-channel image datasets STL-10, CIFAR-10, CIFAR-100 and SUN-397 are given in Table 9. From Table 8 and Table 9 we can observe that our proposed model DMVC-ME significantly outperforms the multi-view baseline (**All-Views**), the corresponding single-view baselines (**S-View-i** and **J-View-i**) and other representative multi-view clustering methods. The experimental results show that our proposed model can generalize well on large scale image datasets. Moreover, our approach also show great superiority over other compared methods when the number of categories is large (see the experiment results on CIFAR-100 and SUN-397). These experimental results fully verify that the joint learning strategy

of multiple deep features, multi-view fusion mechanism and clustering assignment can contribute to more encouraging clustering performance.

References

- [A. Benton 2017] A. Benton, H. Khayrallah, B. G. D. R. S. Z. R. A. 2017. Deep generalized canonical correlation analysis. *arXiv preprint arXiv:1702.02519*.
- [A. Coates and Lee 2011] A. Coates, A. N., and Lee, H. 2011. An analysis of single-layer networks in unsupervised feature learning. In *AISTATS*, 215–223.
- [A. Krizhevsky and Hinton 2012] A. Krizhevsky, I. S., and Hinton, G. E. 2012. Imagenet classification with deep convolutional neural networks. In *NIPS*.
- [B. Xie and Huang 2011] B. Xie, Y. Mu, D. T., and Huang, K. 2011. m-sne: Multiview stochastic neighbor embedding. *IEEE Trans. on Cybernetics* 41:1088–1096.
- [B. Yang and Hong 2017] B. Yang, X. Fu, N. S., and Hong, M. 2017. Towards k-means-friendly spaces: simultaneous deep learning and clustering. In *ICML*.
- [Beck and Teboulle 2009] Beck, A., and Teboulle, M. 2009. Fast gradient-based algorithms for constrained total variation image denoising and deblurring problems. *IEEE Trans. on Image Processing* 18:2419–2434.
- [Blaschko and Lampert 2008] Blaschko, M. B., and Lampert, C. H. 2008. Correlational spectral clustering. In *CVPR*, 1–8.
- [C. Szegedy and Wojna 2015] C. Szegedy, V. Vanhoucke, S. I. J. S., and Wojna, Z. 2015. Rethinking the inception architecture for computer vision. *arXiv preprint arXiv:1512.00567v1*.
- [C. Xu 2015] C. Xu, D. Tao, C. X. 2015. Multi-view self-paced learning for clustering. In *IJCAI*.
- [Dalal and Triggs 2005] Dalal, N., and Triggs, B. 2005. Histograms of oriented gradients for human detection. In *CVPR*.
- [F. Li and Xi 2018] F. Li, H. Qiao, B. Z., and Xi, X. 2018. Discriminatively boosted image clustering with fully convolutional auto-encoders. *Pattern Recognition* 83:161–173.
- [F. Tian 2014] F. Tian, B. Gao, C. Q. C. E. L. T. 2014. Learning deep representations for graph clustering. In *AAAI*, 1293–1299.
- [G. Andrew and Livescu 2013] G. Andrew, R. Arora, J. B., and Livescu, K. 2013. Deep canonical correlation analysis. In *International Conference on Machine Learning*.
- [G. Chao and Bi 2018] G. Chao, S. S., and Bi, J. 2018. A survey on multi-view clustering. *arXiv preprint arXiv:1712.06246v2*.
- [Guo X 2017] Guo X, Liu X, Z. E. e. a. 2017. Deep clustering with convolutional autoencoders. In *ICONIP*, 373–382.
- [Han Xiao 2017] Han Xiao, Kashif Rasul, R. V. 2017. Fashion-mnist: a novel image dataset for benchmarking machine learning algorithms. *arXiv preprint arXiv:1708.07747v2*.
- [Hull 1994] Hull, J. 1994. A database for handwritten text recognition research. *IEEE Trans. Pattern Anal. Mach. Intell.* 16:550–554.
- [J. Deng and Fei-Fei 2009] J. Deng, W. Dong, R. S. L. J. L. K. L., and Fei-Fei, L. 2009. Imagenet: a large-scale hierarchical image databased. In *CVPR*.
- [J. Duchi and Singer 2011] J. Duchi, E. H., and Singer, Y. 2011. Adaptive subgradient methods for online learning and stochastic optimization. *JMLR* 11:2121–2159.
- [J. Xie and Farhadi 2016] J. Xie, R. G., and Farhadi, A. 2016. Unsupervised deep embedding for clustering analysis. In *ICML*, 478–487.
- [J. Yang and Batra 2016] J. Yang, D. P., and Batra, D. 2016. Joint unsupervised learning of deep representations and image clusters. In *CVPR*, 5147–5156.
- [K. Chaudhuri and Sridharan 2009] K. Chaudhuri, S. M. Kakade, K. L., and Sridharan, K. 2009. Multiview clustering via canonical correlation analysis. In *ICML*, 129–136.
- [K. He and Sun 2016] K. He, X. Zhang, S. R., and Sun, J. 2016. Deep residual learning for image recognition. In *CVPR*.
- [Kingma and Ba 2015] Kingma, D. P., and Ba, L. J. 2015. Adam: A method for stochastic optimization. In *International Conference on Learning Representations*.
- [Kingma and Welling 2014] Kingma, D. P., and Welling, M. 2014. Auto-encoding variational bayes. In *International Conference on Learning Representations Workshop*.
- [Krizhevsky and Hinton 2009] Krizhevsky, A., and Hinton, G. 2009. Learning multiple layers of features from tiny images. *Masters Thesis, Department of Computer Science, University of Toronto*.
- [Lowe 2004] Lowe, D. 2004. Distinctive image features from scale-invariant keypoints. *International Journal of Computer Vision* 60:91–110.
- [M. Christopher D. and Schtze 2010] M. Christopher D., P. R., and Schtze, H. 2010. Introduction to information retrieval. *Cambridge University Press* 43:824–825.
- [P. Huang and Wang 2014] P. Huang, Y. Huang, W. W., and Wang, L. 2014. Deep embedding network for clustering. In *International Conference on Pattern Recognition*, 1532–1537.
- [P. Vincent and Manzagol 2010] P. Vincent, H. Larochelle, I. L. Y. B., and Manzagol, P. 2010. Stacked denoising autoencoders: Learning useful representations in a deep network with a local denoising criterion. *Journal of Machine Learning Research* 11:3371–3408.
- [Simonyan and Zisserman 2014] Simonyan, K., and Zisserman, A. 2014. Very deep convolutional networks for large-scale image recognition. In *International Conference on Learning Representations*.
- [T. Kulkarni and Tenenbaum 2015] T. Kulkarni, W. Whitney, P. K., and Tenenbaum, J. 2015. Deep convolutional inverse graphics network. In *Neural Information Processing Systems*.

Table 8: The clustering results on MNIST, fashion-MNIST, USPS and COIL-20.

Method	MNIST			fashion-MNIST			USPS			COIL-20		
	ACC	NMI	ARI	ACC	NMI	ARI	ACC	NMI	ARI	ACC	NMI	ARI
RMKMC	0.8255	0.7995	0.7524	0.5912	0.6169	0.4636	0.7441	0.7278	0.6667	0.5799	0.7487	0.5275
MSPL	0.8717	0.8147	0.7892	0.5607	0.6068	0.4457	0.7414	0.7174	0.6370	0.5992	0.7623	0.5608
DCCA	0.3155	0.2086	0.1272	0.4105	0.4028	0.2342	0.4042	0.3895	0.2480	0.5512	0.7013	0.4600
DCCAE	0.3029	0.2038	0.1274	0.4109	0.3836	0.2303	0.3793	0.3246	0.2135	0.5551	0.7058	0.4667
DGCCA	0.4714	0.3840	0.2789	0.4765	0.4827	0.3105	0.5473	0.5079	0.4011	0.5337	0.6762	0.4370
S-View-1	0.8901	0.8229	0.8034	0.5855	0.6240	0.4610	0.7357	0.7195	0.6363	0.6957	0.7875	0.6200
S-View-2	0.7971	0.6979	0.6545	0.5443	0.5044	0.3721	0.6696	0.6479	0.5716	0.6555	0.7717	0.5922
S-View-3	0.8888	0.8068	0.7888	0.5793	0.6343	0.4632	0.7062	0.6842	0.5813	0.636	0.7607	0.5650
All-Views	0.9062	0.8286	0.8181	0.5993	0.6348	0.4756	0.7367	0.7231	0.6420	0.6737	0.7845	0.6124
J-View-1	0.9378	0.9123	0.9018	0.5982	0.6407	0.4820	0.7831	0.8170	0.7435	0.6870	0.7973	0.6261
J-View-2	0.8929	0.8644	0.8236	0.5886	0.6011	0.4434	0.7465	0.7864	0.6973	0.6675	0.7899	0.6112
J-View-3	0.9071	0.8251	0.8208	0.5462	0.5841	0.4136	0.7610	0.7602	0.6888	0.5597	0.7383	0.4969
DMVC-ME	0.9603	0.9312	0.9316	0.6087	0.6442	0.4864	0.7865	0.8222	0.7480	0.7122	0.8080	0.6524

Table 9: The clustering results on STL-10, CIFAR-10, CIFAR-100 and SUN-397.

Method	STL10			CIFAR10			CIFAR100			SUN397		
	ACC	NMI	ARI	ACC	NMI	ARI	ACC	NMI	ARI	ACC	NMI	ARI
RMKMC	0.7441	0.7278	0.6667	0.5714	0.4688	0.3679	0.2400	0.4100	0.1321	0.2684	0.5049	0.1679
MSPL	0.7414	0.7174	0.6370	0.7156	0.5948	0.5174	0.2330	0.4091	0.1251	0.2704	0.5072	0.1643
DCCA	0.4042	0.3895	0.2480	0.4242	0.3385	0.2181	0.1372	0.2913	0.0594	0.2275	0.4749	0.1257
DCCAE	0.3793	0.3246	0.2135	0.3960	0.3226	0.2034	0.1363	0.2907	0.0596	0.2259	0.4731	0.1236
DGCCA	0.8960	0.8218	0.7970	0.4703	0.3577	0.2634	0.1702	0.3100	0.0734	0.1422	0.3578	0.0635
S-View-1	0.7357	0.7195	0.6363	0.2983	0.1772	0.1024	0.1236	0.2367	0.0437	0.1759	0.4137	0.0842
S-View-2	0.6696	0.6479	0.5716	0.4331	0.3359	0.2243	0.2245	0.3564	0.1059	0.2742	0.5272	0.1760
S-View-3	0.7062	0.6842	0.5813	0.7162	0.5714	0.5013	0.1869	0.3553	0.0904	0.2205	0.4628	0.1186
All-Views	0.7367	0.7231	0.6420	0.7552	0.6069	0.5428	0.2399	0.4110	0.1263	0.2572	0.5108	0.1540
J-View-1	0.7831	0.8170	0.7435	0.3035	0.1832	0.1094	0.1266	0.2334	0.0478	0.1837	0.4116	0.0884
J-View-2	0.7465	0.7864	0.6973	0.4423	0.3447	0.2398	0.2244	0.3569	0.1137	0.2751	0.5198	0.1734
J-View-3	0.7610	0.7602	0.6888	0.7613	0.6424	0.5721	0.1859	0.3573	0.0917	0.2193	0.4645	0.1174
DMVC-ME	0.7865	0.8222	0.7480	0.7954	0.6784	0.6291	0.2513	0.4030	0.1415	0.2884	0.5736	0.1812

[T. Ojala and Maenpaa 2002] T. Ojala, M. P., and Maenpaa, T. 2002. Multiresolution gray-scale and rotation invariant texture classification with local binary patterns. *IEEE Trans. on Pattern Recognition and Machine Intelligence* 24:971–987.

[van der Maaten 2009] van der Maaten, L. 2009. Learning a parametric embedding by preserving local structure. *JMLR* 5:384–391.

[W. Wang and Bilmes 2015] W. Wang, R. Arora, K. L., and Bilmes, J. 2015. On deep multi-view representation learning. In *International Conference on Machine Learning*.

[X. Cai and Huang 2013] X. Cai, F. N., and Huang, H. 2013. Multi-view k-means clustering on big data. In *International Joint Conference on Artificial Intelligence*.

[X. Peng 2016] X. Peng, S. Xiao, J. F. Y. W. Y. Z. 2016. Deep subspace clustering with sparsity prior. In *IJCAI*.

[Xiao J 2010] Xiao J, Hays J, E. K. A. e. a. 2010. Sun database: Large-scale scene recognition from abbey to zoo. In *CVPR*, 3485–3492.

[Y. LeCun and P.Haffner 1998] Y. LeCun, L. Bottou, Y. B., and P. Haffner. 1998. Gradient-based learning applied to document recognition. *Proceedings of the IEEE* 86:2278–2324.